Available online at www.sciencedirect.com
ScienceDirect
Journal of the European Ceramic Society 28 (2008) 539–545
www.elsevier.com/locate/jeurceramsoc

Spark plasma sintering of macroporous calcium phosphate scaffolds from nanocrystalline powders

Faming Zhang [a], Kaili Lin [a], Jiang Chang [a,*], Jianxi Lu [a,b], Congqin Ning [a]

[a] *Biomaterials and Tissue Engineering Research Center, Shanghai Institute of Ceramics, Chinese Academy of Sciences, Shanghai 200050, China*
[b] *Shanghai Bio-lu Biomaterials Co. Ltd., Shanghai 200335, China*

Received 10 February 2007; received in revised form 10 July 2007; accepted 14 July 2007
Available online 14 September 2007

Abstract

Spark plasma sintering (SPS) technique was applied to fabricate macroporous β-tricalcium phosphate (β-TCP) scaffolds from nanocrystalline powders (termed "nano-scaffolds") for bone regeneration applications. The degree of porosity (55–70%) and the macropore size (300–500 μm) of the scaffolds were controlled by modulating the porogen additions. Microstructures with ultrafine grain size (200 nm), increased density of solid matrix, and enhanced neck growth, as well as improved compressive strength and elastic modulus of over 50–100% were achieved in the macroporous nano-scaffolds by SPS in a modified graphite die. The SPS may provide an alternative approach to fabricate macroporous bioceramics nano-scaffolds.
© 2007 Elsevier Ltd. All rights reserved.

Keywords: Sintering; Grain size; Mechanical properties; Calcium phosphate; Biomedical applications; $Ca_3(PO_4)_2$

1. Introduction

Bone regeneration or reconstruction is required in cases involving skeletal defects caused by tumor resection, trauma and abnormalities. β-Tricalcium phosphate (β-TCP) has received great attention as grafts for bone regeneration applications due to its excellent biocompatibility and biodegradability. A porous structure was required for the β-TCP bioceramics using as bone regeneration scaffolds since a porous network allows tissue infiltration and exhibits good osteoconductive capability.[1,2] Despite their favorable biological properties, the poor mechanical properties of the porous β-TCP bioceramics have severely restricted their clinical applications. Some attempts have been used to increase the mechanical strength of porous β-TCP bioceramics, including introducing secondary phase[3,4] and optimizing sintering techniques.[5]

Nanostructured ceramics have exhibited promising mechanical and physical properties, and the fabrication of nanostructured ceramics has already become an exciting prospect in materials research.[6–9] Studies on nanostructured β-TCP bioceramics were mainly focused on nanocrystalline powders[10,11] and solid bioceramics,[12] but few studies were carried out on the fabrication of nanostructured macroporous scaffolds. In respect that the fabrication of nanostructured macroporous β-TCP scaffolds by conventional sintering is frustrated since the presence of high surface and interface area provides a strong driving force for the grain growth. Nanostructure processing has been proved to be quite successful for solid materials,[6,7,12] but little is known about its effectiveness for porous structures.

Spark plasma sintering (SPS) is a comparatively new technique for rapid fabrication of solid nanostructured ceramics, cermets and alloys.[13–16] The problem of grain growth in these nanostructured materials has been overcome to some extent by using SPS with final grain size below 200 nm, even below 100 nm can be achieved.[13,6] Recently, particular attention has been paid on using of SPS to prepare porous ceramics and alloys, for example, alumina,[17–19] aluminum,[20] titanium alloys,[21] etc. Optimized microstructures and improved mechanical properties have been achieved in these porous materials fabricated by SPS. However, the application of SPS to fabricate high porosity macroporous bioceramics scaffolds was scarcely reported. As bone regeneration scaffolds, high porosity (>50%) and macropore size (>200 μm) are essential requirements for osteoconduction.[22,23]

* Corresponding author. Tel.: +86 21 52412804; fax: +86 21 52413903.
E-mail address: jchang@mail.sic.ac.cn (J. Chang).

0955-2219/$ – see front matter © 2007 Elsevier Ltd. All rights reserved.
doi:10.1016/j.jeurceramsoc.2007.07.012

Based on the above analysis, the objective of the present work was emphasized on the fabrication of macroporous β-TCP scaffolds from nanocrystalline powders (termed "nano-scaffolds") using SPS technique with a modified die, which made it possible to eliminate the pressure. The spark plasma sintering behavior, microstructures and mechanical properties of the consolidated macroporous β-TCP nano-scaffolds were investigated and compared with those of conventional pressureless sintered counterparts.

2. Experimental procedure

2.1. Materials

The nanocrystalline β-TCP powders were synthesized by a chemical precipitation reaction. A 0.6 M $Ca(NO_3)_2$ solution was stirred at room temperature, and then was dropped into a stirred 0.4 M $(NH_4)_2HPO_4$ solution to produce calcium phosphate precipitates. The pH of the solution was adjusted to about 8.0 using NH_4OH. The precipitates were dried at 80 °C for 24 h after aging and washing. Finally, the synthesized powders were calcined at 700 and 800 °C for 2 h.

2.2. Preparation procedure

The obtained nanocrystalline β-TCP powders were sieved and mechanically mixed with polyethylene glycol (PEG 6000) particulates (350–650 μm in size) that obtained from Sinopharm Chemical Reagent Co. Ltd., China. The mixtures with 10 wt.% polyvinyl alcohol (PVA) were pressed at 8 MPa uniaxially in a stainless steel die. The porosity of the substrate was adjusted by the amount of PEG. The green disks with a diameter of 10 mm and a thickness of 8 mm were heat-treated at 400 °C for 2 h to remove the organic substances, and then they were presintered at 800 °C for 2 h to obtain strength to handle. The presintered sample was placed into a special graphite die for spark plasma sintering, as illustrated in Fig. 1. A small gap *d* in the range of 1–5 mm was designed to avoid damaging the porous ceramics in the die. The sintering was accomplished using a Model SPS-2040 spark plasma sintering system (Sumitomo Coal Mining Co. Ltd., Japan) at a temperature of 850–1050 °C for various times under a vacuum of 6 Pa. Temperatures were monitored by an optical pyrometer through a non-through hole in the graphite die. The heating rate was maintained as 100 °C/min. For a comparison, the same presintered samples were fabricated by conventional pressureless sintering at 1100 °C for 2 h.

2.3. Characterization

The morphologies of the calcined nanocrystalline β-TCP powders were observed by transmission electron microscopy (TEM, JEM-2010, Japan). X-ray diffraction (XRD, Rigaku D/max 2550V, Japan) was used to characterize the phase composition of the powders and sintered ceramics. The total porosity of the scaffolds was determined by Archimedes method with water as an immersion medium. The average value of five determinations was taken as the total porosity of sintered bodies.

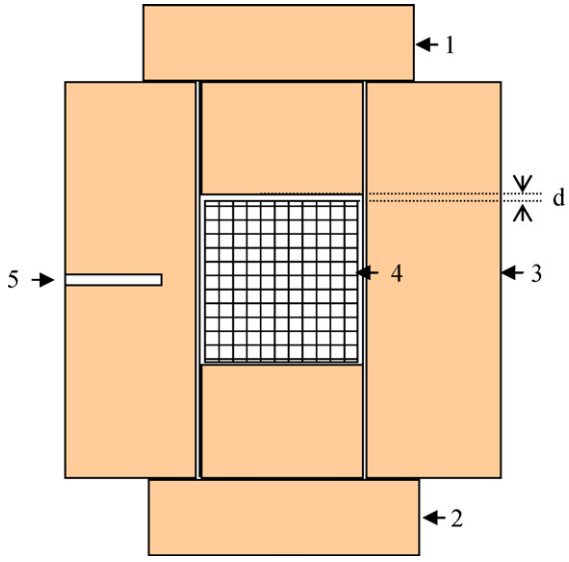

Fig. 1. Schematic diagram of the graphite die for SPS of porous ceramics ((1) top punch, (2) bottom punch, (3) die cavity, (4) porous sample, (5) non-through hole, (*d*) gap).

Microporosity was measured by mercury intrusion method using a PoreMaster 33 porosimeter. SEM analysis of the fractured surfaces of the scaffolds was performed on a scanning electron microscope (SEM, JSM-6700F, Japan). The mean grain size of the porous bioceramics was measured from the high-resolution SEM micrographs of porous walls using an image analyzer. The compressive strength of the scaffolds was measured on a mechanical tester with a 0.5 mm/min crosshead speed (AG-5KN, Shimadzu, Japan). The elastic modulus was calculated from the slope of the initial linear portion of the stress-strain curve. Five samples of each group were used for statistical analysis of the mechanical properties.

3. Results and discussion

3.1. Powder characteristics

The nanocrystalline β-TCP powders were prepared using a chemical precipitation reaction:

$$3Ca(NO_3)_2 + 2(NH_4)_2HPO_4 + 2NH_4OH \rightarrow Ca_3(PO_4)_2\downarrow + 6NH_4NO_3 + 2H_2O \quad (1)$$

After precipitation, the precipitates were washed, dried and calcined. Fig. 2 shows the X-ray diffraction patterns of the precursors and calcined calcium phosphate powders at different temperatures. Low-crystalline Ca-deficient apatite (CDHA) phase (ICDD No. 46-905) was observed in the precipitated precursors (Fig. 2a). The CDHA with chemical formula of $Ca_9HPO_4(PO_4)_5OH$ has an apatite structure with peak positions matching closely to the diffraction peaks of stoichiometric hydroxyapatite (ICDD No. 09-432). The wet-chemical method for β-TCP synthesis was most commonly used to form the CDHA precursors with Ca/P molar ratio (1.50), which is the same as that in β-TCP.[10] After calcined at 700 °C, partial CDHA

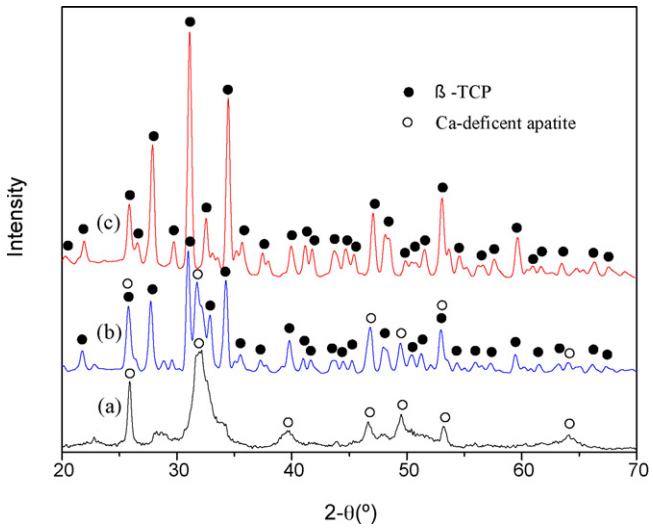

Fig. 2. X-ray diffraction patterns of the precursors (a) and calcined calcium phosphate powders at 700 °C (b) and 800 °C (c).

has been transformed into the β-whitlockite (β-TCP) phase (Fig. 2b). But some CDHA was still preserved (Fig. 2b). Pure crystalline β-TCP phase (ICDD No. 09-169) formed after calcined at 800 °C (Fig. 2c). The transformation from Ca-deficient apatite to β-TCP is described by the following equation[10]:

$$Ca_9HPO_4(PO_4)_5OH \rightarrow 3Ca_3(PO_4)_2 + H_2O \quad (2)$$

It was reported the above phase transformation temperature is 790 °C in the calcium phosphate precipitates.[24] Therefore, 800 °C was chosen as the calcination temperature of the chemical precipitates to obtain a pure β-TCP phase. The typical TEM morphology of the nanocrystalline β-TCP powders that calcined at 800 °C is shown in Fig. 3. The mean particle size of the particulates was about 80 nm. The powders were spherical in shape and there were some agglomerates in the powders. The selected area electron diffraction (SAED) pattern (inset) of one nano-particle was indexed as [1$\bar{1}$0] zone axis of the β-whitlockite.

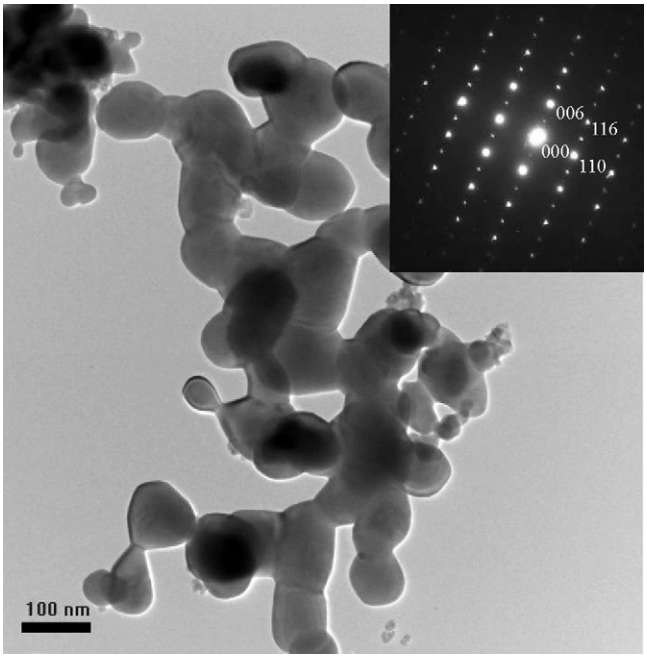

Fig. 3. TEM micrograph of the nanocrystalline β-TCP powders with corresponding SAED pattern (inset).

3.2. Spark plasma sintering behavior

The sintering behavior of the nanocrystalline β-TCP powders during SPS was studied. It is found that solid β-TCP bioceramics could be fabricated from nanocrystalline powders by SPS at a temperature of 880 °C for 3 min and axial pressures of 50 MPa. The relative density was 99% determined by Archimedes method. However, the porous β-TCP bioceramics nano-scaffolds need much higher temperature for a high density. As presented in Fig. 4, the total porosity decreased with the increase of temperature and holding time. At temperature of 950 °C for 5 min, it achieved a stable porosity of 66 ± 1.0%. The total porosity decreased marginally when the temperature increased above 1000 °C. As a result, high-density β-TCP nano-scaffolds were fabricated at 950 °C for 5 min by SPS. The XRD pattern result shows that the original β-TCP phase was preserved and no high temperature phase (α-TCP) was detected in the β-TCP scaffolds after spark plasma sintered at 950 °C for 5 min (Fig. 5).

The spark plasma sintering furnace was modified for preparation of macroporous scaffolds, where the presence of a gap *d* in the die (Fig. 1) resulted in a pressureless environment for the sample. The driving force for sintering of the porous bioceramics was just provided by the surface energy of the nano-particles. Therefore, higher sintering temperature (950 °C) was needed in SPS of the macroporous β-TCP scaffolds compared with the solid bioceramics (880 °C) from nanocrystalline powders. In contrast, the sintering temperature of the β-TCP scaffolds from the same nanocrystalline powders was 1100 °C by the conventional pressureless sintering. This difference in the sintering temperature may be due to the sintering effects of pulsed direct current field. The particles that were activated during SPS led to a decrease of sintering temperature. It also may due to the temperature difference between the measured

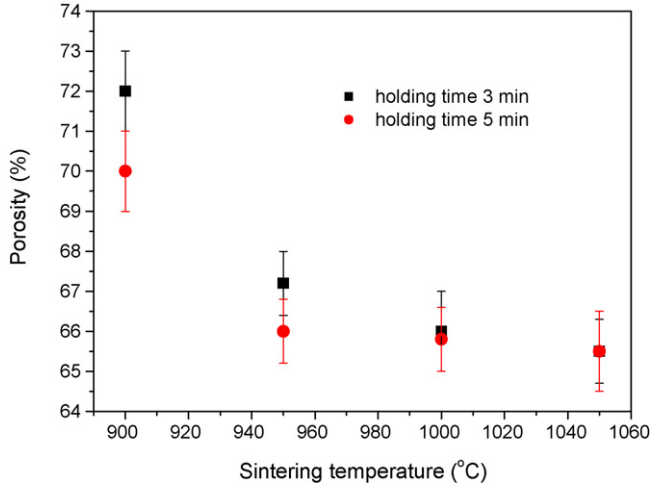

Fig. 4. Variation of scaffolds porosity with SPS temperature.

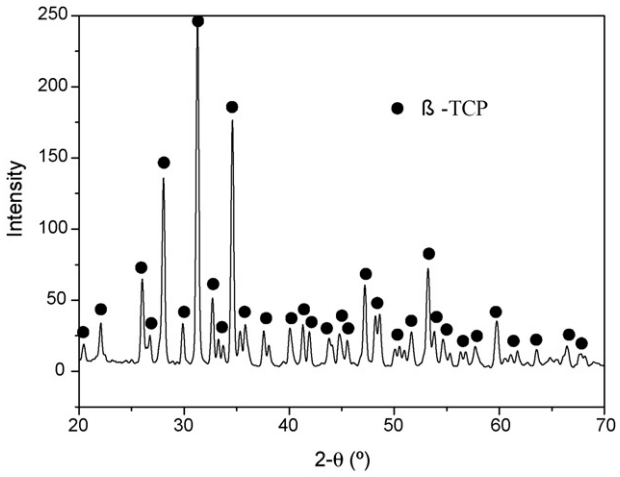

Fig. 5. X-ray diffraction pattern of spark plasma sintered β-TCP scaffolds.

and actual temperature in SPS which sometime rises to above 100 °C.

3.3. Microstructures

The SEM micrographs of macroporous β-TCP scaffolds prepared by SPS and conventional sintering are shown in Fig. 6. The macroporous structure of the spark plasma sintered scaffolds seems smooth, while the conventional sintered counterpart seems rough (Fig. 6a and b). The shapes and sizes of the pores were similar to those of the PEG particulates. The scaffolds showed macropore sizes ranging from 300 to 500 μm. A pore size greater than 200 μm are essential requirements for osteoconduction.[22,23] The optimal pore size for attachment, differentiation, and growth of osteoblasts and for vascularization is approximately 300–400 μm.[25,26]. Thus, the macropore size in the β-TCP scaffolds meets the requirements for osteoconduction and bone regeneration. Then, the morphologies of pore walls were examined (Fig. 6c–f). The grains were well interconnected by the formation of almost melted, thick and strong necks with minimal grain growth in the spark plasma sintered scaffolds (Fig. 6e). The mean grain size, measured from SEM image using an image analyzer, in the spark plasma sintered scaffolds was about 200 nm (Fig. 6c and e), while that in the conventional sintered scaffolds was about 1.0 μm (Fig. 6d and f). The spark plasma sintered scaffolds showed enhanced neck growth, and refined grain size compared to the conventional sintered ones.

In order to identify the microporosity and micropores distribution, mercury intrusion method was employed for the scaffolds sintered by the two techniques. The samples for the mercury intrusion measurement expressed the same total porosity of 66 ± 1.0% determined by Archimedes methods. Microporosity is defined as pore sizes less than 10 μm.[27] Fig. 7 shows the mercury intrusion volume versus micropore diameter of the spark plasma sintered and conventional sintered β-TCP scaffolds. Microporosity of the scaffolds was calculated statistically from the mercury intrusion volume. The microporosity of the spark plasma sintered scaffolds (1.8 ± 0.3 vol.%) was much lower than that of the conventional sintered scaffolds (8.0 ± 0.2 vol.%). As noted in Fig. 7, the distribution of micropore diameter mainly ranged from several nanometers to about 3.0 μm in the spark plasma sintered scaffolds. In contrast, the micropore diameter was mainly distributed from 4.0 to 9.5 μm in the conventional sintered scaffolds. The spark plasma sintered scaffolds showed lower microporosity and smaller micropores than that of the conventional sintered counterparts. From the SEM results in Fig. 6c–f, it is noticed that there were fewer micropores in pore walls of the spark plasma sintered scaffolds than those of the conventional sintered counterparts. Additionally, the average size of micropores in the spark plasma sintered and conventional sintered scaffolds were around 100 nm and several μm, respectively. Thus, the microporosity measurement results by mercury intrusion method (Fig. 7) were consistent with the SEM analysis (Fig. 6c–f). The macroporosity is the result of total porosity subtracted microporosity. The spark plasma sintered scaffolds possessed higher macroporosity than that of conventional sintered counterparts. The SPS has led to a lower microporosity and smaller micropores in the scaffolds without loss of macroporosity, which contribute to the increase in the density of the solid matrix.

3.4. Mechanical properties

Fig. 8 shows the mechanical properties variation of the macroporous β-TCP scaffolds as a function of porosity. Both the compressive strength and elastic modulus of the composites decreased as the porosity increased. After fit testing, it is found that the relationship between the porosity and mechanical properties of the porous scaffolds obeys exponential decay equation, which are in accordance with the function that proposed by Rice.[28] The compressive strength and elastic modulus of the spark plasma sintered scaffolds with 66 ± 1.0% porosity were 3.1 ± 0.4 and 48.5 ± 8 MPa, respectively. In contrast, the compressive strength of the conventional sintered scaffolds with the same porosity was only 1.6 ± 0.5 MPa and the elastic modulus was only 31.2 ± 6 MPa. At porosity 55 ± 1.0%, the spark plasma sintered scaffolds showed a compressive strength of 7.0 ± 0.8 MPa and an elastic modulus of 240.5 ± 20 MPa, but the conventional sintered scaffolds exhibited a compressive strength of 4.8 ± 0.5 MPa and an elastic modulus of 150.2 ± 25 MPa. As expected, the spark plasma sintered scaffolds exhibited much higher mechanical properties than the conventional sintered counterparts. The spark plasma sintered nano-scaffolds provide improved mechanical properties, which are about 50–100% higher than those of the conventional sintered scaffolds with porosity from 55 to 70%.

The improved mechanical properties of spark plasma sintered scaffolds were due to their microstructure optimization evidenced by the refinement of grain size, the increment of matrix density, and the enhancement of neck growth. Refining grain size of a solid ceramic is a well-known method to achieve improved mechanical properties. The reducing in grain size results in a mechanical strength increase in solid materials. The solid nanostructured ceramics and metals have been extensively studied and exhibited excellent mechanical properties.[13–16] However, the preparation of nanostructured porous scaffolds is a great

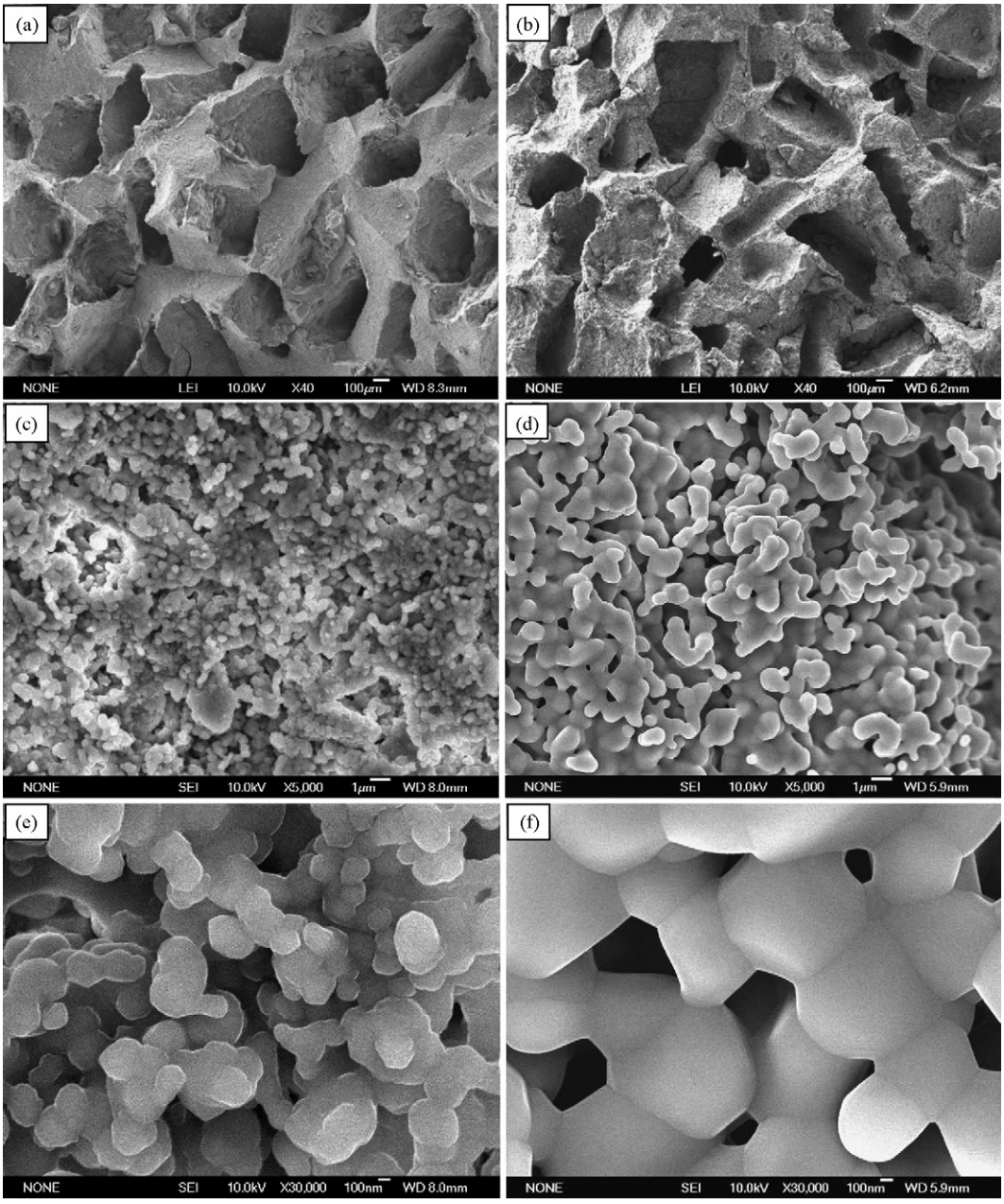

Fig. 6. SEM micrographs of the macroporous β-TCP scaffolds fabricated by SPS (a, c, e) and conventional sintering (b, d, f) showing the macroporous structure and pore walls.

challenge since nanocrystals have a rapid grain growth. Some researches tried to fabricate porous ceramics by SPS using a relative low pressure, for instance 5 MPa.[17,18] Unfortunately, the porosity is less than 50% and the pore size is not controllable. In this study, the graphite die was designed with a small gap *d* to eliminate the pressure for SPS of high porosity macroporous nano-scaffolds. The porosity of the scaffolds was controlled in the range of 55–70% and the macropore size was modulated in the range of 300–500 μm by porogen additions. The experimental results showed that SPS also could be used to fabricate high porosity macroporous bioceramics nano-scaffolds by the special die design. The grain growth of nanocrystals has been inhibited to some extent by SPS, as a result ultrafine grain sized (200 nm) β-TCP scaffolds were fabricated. There are more the number of necks per unit volume that drives the strength in the macroporous ceramics. Thus, the mechanical properties of porous nano-scaffolds were increased accordingly. The nanostructure processing is also effective for porous structures.

The density of the solid matrix related to the microporosity and micropore sizes is an important factor tending to influence the mechanical properties of the porous ceramics. The spark plasma sintered scaffolds showed a lower microporosity and smaller micropore sizes, which led to a higher density of the solid matrix without loss of macroporosity (Fig. 7). Microporosity is dominated by some critical parameters, such as the original particle size, sintering temperature and holding time.

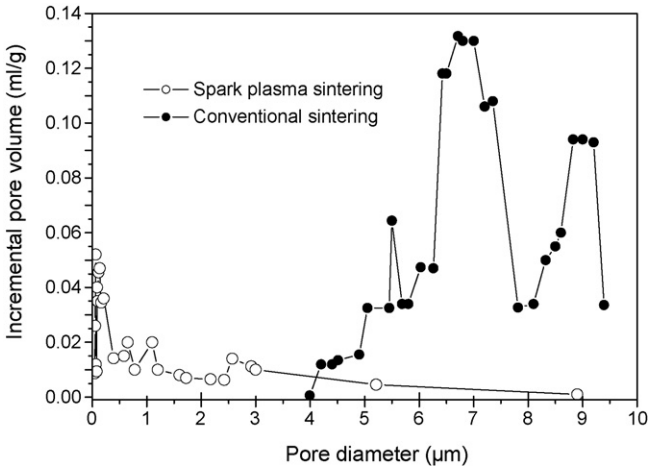

Fig. 7. Variation of mercury intrusion volume vs. micropore diameter of the β-TCP scaffolds fabricated by SPS and conventional sintering.

Since the scaffolds prepared at different conditions were sintered from the same β-TCP nanocrystalline powders, the SPS technique plays the key role for the decrease of microporosity and micropore sizes in the β-TCP scaffolds. These micropores are located between ceramic grains after the materials were sintered. Microporosity could allow body fluid circulation whereas macroporosity provides space for bone-cell colonization.[27] The micropores are not beneficial to the bone tissue ingrowths; however, they have significant effects on the mechanical properties, degradation rate, and surface properties of bioceramic scaffolds.[29–31]

There was no axial pressure on the sample, but the neck growth of grains was greatly enhanced to almost a melted state in the SPS process. It was attributed to the rapid heating between the activated particles and the enhanced diffusion in the pulsed dc electric field resulting in a better sintering effect. During SPS, the discharge that is assumed to take place in voids between particles is thought to promote the particles bridging by neck growth in the initial stage of sintering.[18] The diffusion in SPS can be formulated as follows

$$\frac{\partial n}{\partial t} = D\frac{\partial^2 n}{\partial x^2} + \mu E\frac{\partial n}{\partial x} \quad (3)$$

where n is the atom numbers of diffusion, t the sintering time, D the diffusion coefficient, E the electric intensity, x the diffusion distance and μ is the atom displacement in electric field. Owing to the effect of spark activation in SPS, the D-value was greatly enhanced. Moreover, electric field E was added in Eq. (3). Subsequently, the neck growth was enhanced by the incremental diffusion over densification in SPS. The enhanced diffusion in SPS plays a dominate role in promoting the neck growth of grains. The formation of necks between grains by surface diffusion before densification can significantly improve the mechanical strength and elastic modulus of dense and porous materials. Consequently, the improvement in mechanical properties of the nano-scaffolds by SPS was attributed to the reducing of grain size, the increment of density in the solid matrix, and the enhanced neck growth of grains.

In this study, improved compressive strength and elastic modulus of porous β-TCP scaffolds were obtained by SPS of the nanocrystalline powders. The final grain size in the scaffolds was above 100 nm primarily due to the grain size of initial nanocrystalline powders was just below 100 nm. Although the grain size of the spark plasma sintered nano-scaffolds (200 nm) was not in the nanometer scale, their mechanical properties were much higher than those of the conventional sintered scaffolds (1 μm). This indicated that the nanostructure processing is also effective for porous structures. Actually, the mechanical properties in these spark plasma sintered nano-scaffolds are still low. Factors tending to influence the mechanical properties of the β-TCP nano-scaffolds may be due to the non-uniform electric field and rapid cooling rate during SPS resulting in some residual stress preserved in the porous scaffolds, as well as the decomposition, distribution and shape of the PEG porogens, which need further investigation. It is believed that the mechanical properties of the β-TCP scaffolds could be further improved by refining grain size to nanometer scale, and optimizing the pore form-

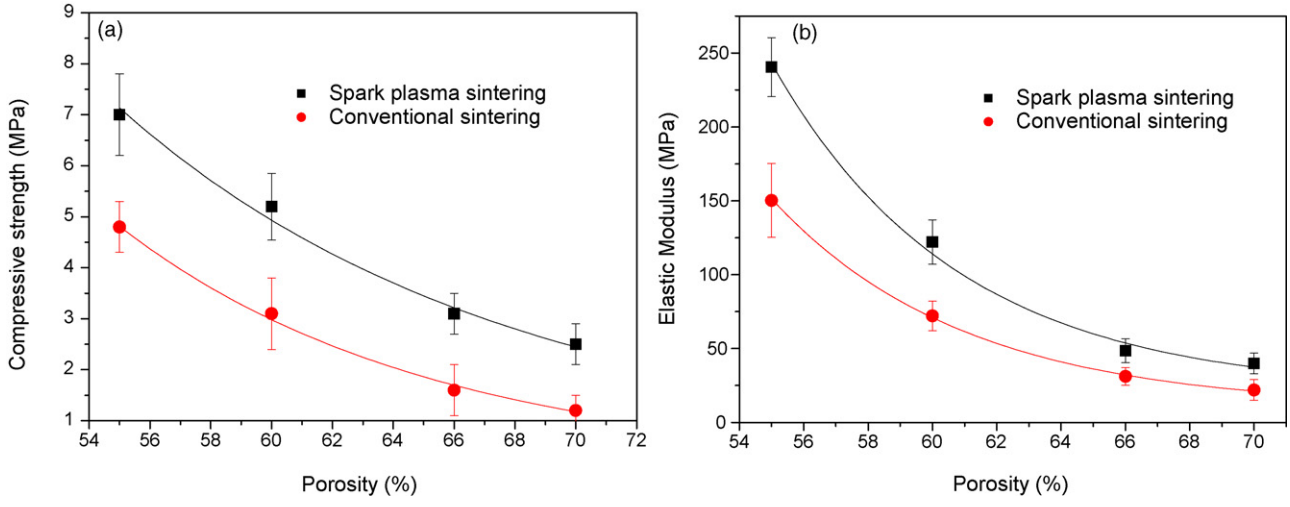

Fig. 8. Compressive strength (a) and elastic modulus (b) of the β-TCP scaffolds fabricated by SPS and conventional sintering.

ing techniques. Despite all that, this study has indicated that the SPS can be used to fabricate high porosity macroporous bioceramics nano-scaffolds by the special die design. The grain growth of nanocrystals was inhibited by SPS, and the mechanical properties of porous bioceramics were increased accordingly. The SPS technique may provide a new method for fabricating macroporous bioceramics nano-scaffolds.

4. Conclusions

Macroporous scaffolds were successfully fabricated from nanocrystalline β-TCP powders by using SPS technique with a modified die. The degree of porosity (55–70%) and the macropore size (300–500 μm) of the scaffolds were controlled by modulating the porogen additions. The SPS could inhibit the grain growth of nanocrystals, increase the density of the solid matrix, and enhance the neck growth of grains, as well as improve the compressive strength and elastic modulus (50–100%) of the macroporous nano-scaffolds. The SPS seems to provide an alternative approach to fabricate macroporous bioceramics nano-scaffolds.

Acknowledgments

We thank the China Postdoctoral Science Foundation (No. 20060390648), Shanghai Postdoctoral Scientific Key Program (No. 06R214201), the Science & Technology Commission of Shanghai Municipality (No. 05JD14005, No. 05DZ05034) and state 973 Program of China (No. 2005CB522704) for the financial supports.

References

1. Shimizu, T., Zerwekh, J. E., Videman, T., Gill, K., Mooney, V., Holmes, R. E. *et al.*, Bone ingrowth into porous calcium phosphate ceramics: influence of pulsing electromagnetic field. *J. Orthopaedic Res.*, 1988, **6**(2), 248–258.
2. Radin, S. R. and Ducheyne, P., Effect of bioactive ceramic composition and structure on in vitro behavior. III. Porous versus dense ceramics. *J. Biomed. Mater. Res.*, 1994, **11**(28), 1303–1309.
3. Ramay, H. R. R. and Zhang, M., Biphasic calcium phosphate nanocomposite porous scaffolds for load-bearing bone tissue engineering. *Biomaterials*, 2004, **25**, 5171–5180.
4. Samar, J. K., Himesh, A. B. and Dhamne, A., $MgO–Na_2O–P_2O_5$ based sintering additives for tricalcium phosphate bioceramics. *J. Am. Ceram. Soc.*, 2006, **89**, 5–881.
5. Wang, X., Fan, H., Xiao, Y. and Zhang, X., Fabrication and characterization of porous hydroxyapatite/β-tricalcium phosphate ceramics by microwave sintering. *Mater. Lett.*, 2006, **60**, 455–458.
6. Anselmi-Tamburini, U., Garay, J. E. and Munir, Z. A., Fast low-temperature consolidation of bulk nanometric ceramic materials. *Scripta Mater.*, 2006, **54**, 823–828.
7. Edward, S. A., Nathaniel, J. G., Atsushi, N. and Jackie, Y. Y., Nanostructure processing of hydroxyapatite-based bioceramics. *Nano Lett.*, 2001, **1**, 149–153.
8. Chevalier, J., Deville, S., Fantozzi, G., Bartolome, J. F., Pecharroman, C., Moya, J. S. *et al.*, Nanostructured ceramic oxides with a slow crack growth resistance close to covalent materials. *Nano Lett.*, 2005, **5**, 1297–1301.
9. Bellino, M. G., Lamas, D. G. and Walsoe de Reca, N. E., Enhanced ionic conductivity in nanostructured, heavily doped ceria ceramics. *Adv. Funct. Mater.*, 2006, **16**, 107–113.
10. Bow, J. S., Liou, S. C. and Chen, S. Y., Structural characterization of room-temperature synthesized nano-sized β-tricalcium phosphate. *Biomaterials*, 2004, **25**, 3155–3161.
11. Prashant, N. K., Charles, S., Lee, D. H. and Olton, D., Nanostructured calcium phosphates for biomedical applications: novel synthesis and characterization. *Acta Biomater.*, 2005, **1**, 65–83.
12. Lin, K. L., Qin, C., Ni, S. Y., Chen, L. D., Lu, J. X. and Chang, J., Fabrication of transparent $\beta\text{-}Ca_3(PO_4)_2$ bioceramics by spark plasma sintering technique using ultrafine powders. *J. Inorg. Mater.*, 2006, **21**, 645–650 [in Chinese].
13. Lee, Y. I., Lee, J. H., Hong, S. H. and Kim, D. Y., Preparation of nanostructured TiO_2 ceramics by spark plasma sintering. *Mater. Res. Bull.*, 2003, **38**, 925–930.
14. Kumar, R., Prakash, K. H., Cheang, P. and Khor, K. A., Microstructure and mechanical properties of spark plasma sintered zirconia-hydroxyapatite nano-composite powders. *Acta Mater.*, 2005, **53**, 2327–2335.
15. Zhang, F. M., Shen, J. and Sun, J. F., Processing and properties of carbon nanotubes-nano-WC-Co composites. *Mater. Sci. Eng. A*, 2004, **381**, 86–91.
16. Yoritoshi, M., Yuichiro, K., Nobuhiro, T., Naoko, H., Kiyoshi, M. and Yoshihira, O., Microstructures and mechanical properties of bulk nanocrystalline Fe–Al–C alloys made by mechanically alloying with subsequent spark plasma sintering. *Sci. Technol. Adv. Mater.*, 2004, **5**, 133–143.
17. Oh, S. T., Tajima, K. I., Ando, M. and Ohji, T., Strengthening of porous alumina by pulse electric current sintering and nanocomposite processing. *J. Am. Ceram. Soc.*, 2000, **83**, 1314–1316.
18. Jayaseelan, D. D., Kondo, N. M., Brito, E. and Ohji, T., High-strength porous alumina ceramics by the pulse electric current sintering technique. *J. Am. Ceram. Soc.*, 2002, **85**, 267–269.
19. Cho, W. S., Yoo, Y. C., Whang, C. M., Cho, N. H., Kim, J. G., Kwon, Y. J. *et al.*, Preparation of porous alumina ceramics by spark plasma sintering. *Ceram. Trans.*, 2006, **194**, 73–82.
20. Hakamada, M., Yamada, Y., Nomura, T., Chen, Y., Kusuda, H. and Mabuchi, M., Fabrication of porous aluminum by spacer method consisting of spark plasma sintering and sodium chloride dissolution. *Mater. Trans.*, 2005, **46**, 2624–2628.
21. Asaoka, K. and Kon, M., Sintered porous titanium and titanium alloys as advanced biomaterials. *Mater. Sci. Forum*, 2003, **426–432**, 3079–3084.
22. Liu, D. M., Influence of porosity and pore size on the compressive strength of porous hydroxyapatite ceramic. *Ceram. Int.*, 1997, **23**, 135–139.
23. Jaw, K. S., Preparation of a biphasic calcium phosphate from $Ca(H_2PO_4)_2{\cdot}H_2O$ and $CaCO_3$. *J. Thermal Anal. Calorim.*, 2006, **83**, 145–148.
24. Gibson, I. R., Rehman, I., Best, M. S. and Bonfield, W., Characterization of the transformation from calcium-deficient apatite to β-tricalcium phosphate. *J. Mater. Sci. Mater. Med.*, 2000, **12**, 799–804.
25. Tsuruga, E., Takita, H., Itoh, H., Wakisaka, Y. and Kuboki, Y., Pore size of porous hydroxyapatite as the cell-substratum controls BMP-induced osteogenesis. *J. Biochem.*, 1997, **121**, 317–324.
26. Masanori, O., Yoshiko, D., Hajime, O., Hideki, S., Masako, I., Asako, M. *et al.*, Influence of the porosity of hydroxyapatite ceramics on *in vitro* and *in vivo* bone formation by cultured rat bone marrow stromal cells. *J. Mater. Sci. Mater. Med.*, 2006, **17**, 327–336.
27. Le Guéhennec, L., Layrolle, P. and Daculsi, G., A review of bioceramics and fibrin sealant. *Eur. Cells Mater.*, 2006, **8**, 1–11.
28. Rice, R. W., Comparison of stress concentration versus minimum solid area based mechanical property–porosity relations. *J. Mater. Sci.*, 1993, **28**(8), 2187–2190.
29. Bignon, A., Chouteau, J., Chevalier, J., Factozzi, G., Carret, J. P., Chavassieux, P. *et al.*, Effect of micro- and macroporosity of bone substitutes on their mechanical properties and cellular response. *J. Mater. Sci. Mater. Med.*, 2003, **14**, 1089–1097.
30. Klein, C. P. A. T., Driessen, A. A., de Groot, K. and van den Hooff, A., Biodegradation behavior of various calcium phosphate materials in bone tissue. *J. Biomed. Mater. Res.*, 1983, **17**(5), 769–784.
31. Habibovic, P., Yuan, H., Van Der Valk, C. M., Meijer, G., Van Blitterswijk, C. A. and De Groot, K., 3D microenvironment as essential element for osteoinduction by biomaterials. *Biomaterials*, 2005, **26**(17), 3565–3575.